

Universal behavior of magnon-mediated spin transport in disordered NM/NM/FI heterostructure

Gaoyang Li,¹ Fuming Xu,¹ and Jian Wang^{1,2,*}

¹College of Physics and Optoelectronic Engineering, Shenzhen University, Shenzhen 518060, China

²Department of Physics, University of Hong Kong, Pokfulam Road, Hong Kong, China

We numerically investigate the magnon-mediated spin transport and scaling behaviors of a nonmagnetic metal/nonmagnetic metal/ferromagnetic insulator (NM/NM/FI) heterostructure in the presence of Anderson disorders. For the two-dimensional (2D) NM/NM/FI system, an enhancement of spin conductance in the weak disorder regime is found due to the increasing of the interfacial density of states (DOS) at NM/FI interface. As a result, a new scaling regime is uncovered in the metallic regime where the spin conductance fluctuation rms(G_T) scales linearly with the average spin conductance $\langle G_T \rangle$, independent of system parameters such as Fermi energies and temperatures. The competition between the disorder-enhanced interfacial DOS and disorder-suppressed spin transport results in a non-monotonic dependence of average spin conductance on disorder strength. In the localized regime, the variance of $\ln G_T$ for different system parameters follows a universal function that depends linearly on the average of logarithm of spin conductance $\langle \ln G_T \rangle$. The distribution of $\ln G_T$ in the localized regime is non-Gaussian whose deviation from Gaussian can be characterized by the third and fourth order cumulants of $\ln G_T$, denoted as k_3 and k_4 , respectively. We find that $k_3 \sim \langle -\ln G_T \rangle^{3/2}$ and $k_4 \sim \langle \ln G_T \rangle^2$. These scaling behaviors are different from that of charge conductance in 2D normal metallic systems. This suggests that the spin conductance mediated by magnon in NM/NM/FI hybrid systems belongs to a different universality class. For fixed $\langle \ln G_T \rangle$, the $\ln G_T$ distribution in the localized regime for different system parameters (Fermi energy and temperatures) is found to collapse onto a single curve, suggesting the distribution $P(\ln G_T; \langle \ln G_T \rangle)$ is a universal function that depends only on $\langle \ln G_T \rangle$. Furthermore, spin thermopower S in the presence of disorder is studied and the variance of $\ln S$ is found to scale linearly with $\langle \ln S \rangle$ for different system parameters in the localized regime. Spin conductance and spin thermopower for 1D NM/NM/FI are also studied. Our numerical results suggest that the statistical behaviors of spin conductance mediated by magnon is similar to that of charge conductance in 1D normal systems.

I. INTRODUCTION

Anderson localization¹, a basic concept in condensed-matter physics, describes the process that a phase coherent transport being completely suppressed by introducing disorder. It's the common belief that in the presence of weak disorders, the wave functions of conduction electrons are extended. While for strong disorders, the wave functions localize exponentially^{2,3}. The extended states in band center and the localized states in band tails are separated by the mobility edges proposed by Mott⁴. Due to the crossing of mobility edges, the metal-insulator transition (MIT) occurs at a critical disorder strength W_c . The theory of single-parameter scaling (SPS)^{2,5-10} as well as other important works¹¹⁻¹⁹ serves as a foundation of our understanding of MIT in disordered systems. It's now understood⁷ that scaling in Anderson localization must be considered in terms of the full distribution of conductance. The SPS hypothesis states that the conductance distribution has a universal form, which is fully determined by a single parameter, the ratio of system size L to the localization length ξ . The localization length is obtained from the average of the logarithm of the conductance G while increasing the system size L :

$$\frac{1}{\xi} = - \lim_{L \rightarrow \infty} \frac{1}{2L} \langle \ln G \rangle. \quad (1)$$

Consequently, the average of the logarithm $\langle \ln G \rangle$ is usually used for the numerical verification of SPS in localized regime²⁰⁻²², since one does not have to calculate the localization length.

The validity of SPS in one-dimensional (1D) normal sys-

tems has been thoroughly checked analytically and numerically²³⁻³¹. It was shown that the distribution of $\ln G$ approaches a Gaussian form in the localization limit, which is fully determined by two parameters, i.e., the mean $\langle \ln G \rangle$ and the variance of $\ln G$. The variance of $\ln G$ is defined as $\sigma^2(\ln G) = \langle \ln^2 G \rangle - \langle \ln G \rangle^2$. Both parameters are related to each other through a universal law^{7,28,29}

$$\sigma^2(\ln G) = A \langle -\ln G \rangle^n + B, \quad (2)$$

in which the exponent n equals to 1. Eq. (2) reduces the two parameters of distribution to one and justifies the SPS in 1D systems. In the metallic regime at weak disorders, the distribution function of conductance is found to be Gaussian²⁹. The situation in 2D is more complicated. Most numerical investigations are in agreement with SPS^{20,22,32-38}, although some deviations were reported^{21,39,40}. Prior *et al.*²⁰ numerically confirmed that universal relation Eq.(2) holds in a large region from the diffusive to localized regime and the exponent $n = 2/3$ ⁴¹. The histogram of $\ln G$ was found to approach Tracy-Widom distribution in the localized limit^{20,35,38}. But for Fermi energies near the band edge, SPS breaks down. In a disordered graphene nanoribbon (quasi-1D system)²¹, numerical calculations found $n = 1$, but Eq. (2) is not universal in the entire energy spectrum. So for this system, the SPS hypothesis fails and a second parameter, characteristic distance between states, is needed to scale different disorder strengths.

Besides the charge transport, magnon-based spin transport phenomena have attracted great interest in the field of insulator spintronics in recent years⁴². In these magnetic insulators, band structure does not allow electron transport, but the pure spin current can be carried by a collective mode called spin

wave or magnon. Experimentally, the magnon spin current is generated via spin pumping^{43–46} driven by ferromagnetic resonance or spin Seebeck effect (SSE)^{47–52} and detected in another nonmagnetic metal (NM) via inverse spin Hall effect. The most popular structure is the bilayer structure Pt/YIG. Pt is a heavy metal with strong spin-orbit coupling, and YIG is a ferromagnetic insulator (FI) with long propagating distance of spin wave. SSE in magnetic insulators has been studied both theoretically^{51,53,54} and experimentally^{48,55–57}. Spin rectification and negative differential SSE are also discussed⁵⁸.

Anderson localization of magnonic spin transport in 1D magnetic insulator is studied recently^{59,60}. It was found that disorder suppresses the transmission probability, and Eq. (1) still holds. Although Anderson localization of charge transport in normal metallic systems and magnonic spin transport in ferromagnetic insulators have been investigated, the theoretical investigation of scaling properties of spin transport mediated by magnon in the NM/NM/FI hybrid system remains untouched. Due to the presence of temperature bias and electron-magnon coupling at the interface, one may obtain different transport and scaling behaviors from that of noninteracting electron systems. Using the non-equilibrium Green's function (NEGF) formalism we developed⁶¹ and adding disorder on central NM region, we are able to investigate the magnon-mediated spin transport properties and Anderson localization in NM/NM/FI hybrid systems. Our results suggest that the statistical property of spin conductance mediated by magnon in 2D belongs to a different universality class from that of charge transport in normal systems.

For 2D NM/NM/FI system our results can be summarized as follows. (1) Usually, the charge and spin conductance decrease monotonically with the disorder strength. For the spin conductance mediated by magnon, the average spin conductance is enhanced in the weak disorder regime and suppressed in strong disorders. The non-monotonic behavior is the consequence of competition between disorder-enhanced interfacial density of states (DOS) and disorder-suppressed spin transport. This effect provides a new way of thinking in enhancing the spin transport since much efforts have been paid experimentally to achieve a larger spin Seebeck coefficient by inserting intermediate layers^{62–70} or changing surface roughness⁶³. As a consequence of this enhancement, we unveil a new scaling regime that does not exist in the charge and spin transport in normal metallic systems: the spin conductance fluctuation $\text{rms}(G_T)$ scales linearly with the average spin conductance in the metallic regime, independent of system parameters such as temperatures and Fermi energies. (2) As one of the Hallmarks in the mesoscopic systems, the charge conductance fluctuation exhibits universal behavior in the diffusive regime, which is the focus of numerous studies. For spin transport mediated by magnon, spin fluctuation is found to have similar behavior as that of the charge transport for individual system parameters in 2D NM/NM/FI hybrid systems. However, the spin fluctuations versus disorder strength for different system parameters do not collapse into a single curve, i.e., the spin fluctuation depends on the system parameters and thus is not universal. (3) Furthermore, we study the evolution of spin conductance distribution as we change the disorder strength W . Largely

speaking, 2D spin conductance distributions look similar to that of charge transport in the corresponding regimes. (4) Moreover, we examine the universal behaviors of spin conductance when varying different system parameters in 2D. We find that $\langle \ln G_T \rangle$ versus disorder strength W collapse into a single universal curve for different system parameters in the whole range of W which covers metallic, diffusive, and localized regimes. In addition, we reveal that the variance of $\ln G_T$ scales linearly with $\langle \ln G_T \rangle$ in the diffusive and localized regimes, independent of system parameters. Note that for charge transport in normal systems, the scaling exponent is $2/3$ in localized regime instead of 1 found here. (5) For higher order correlations, we find that the skewness, kurtosis, the third and fourth order cumulants of $\ln G_T$ versus $\langle \ln G_T \rangle$ also exhibit universal behaviors in all regimes, i.e., metallic, diffusive, and localized regimes. In particular, the fourth order cumulant of $\ln G_T$, κ_4 , is found to be a quadratic function of $\langle \ln G_T \rangle$ in all regimes, independent of system parameters. In addition, we find $\kappa_3 \sim \langle -\ln G_T \rangle^{3/2}$ in the localized regime and $\kappa_3 \sim \langle \ln G_T \rangle$ in the diffusive regime. Note that the universal behaviors of third and fourth order cumulants for charge transport have been investigated before in the localized regime with the following result: $\kappa_3 \sim \langle -\ln G \rangle$ and $\kappa_4 \sim \langle -\ln G \rangle^{4/3}$ in 2D normal metallic systems, where G is charge conductance. (6) The distribution of $\ln G_T$ in the localized regime also exhibits universal behavior. Specifically, we find that the distribution function $P(\ln G_T, \langle \ln G_T \rangle)$ is a universal function that depends only on $\langle \ln G_T \rangle$ and not on the other system parameters. (7) We also investigate the spin thermopower S in the presence of disorders. In the localized regime, it is found that the variance of $\ln S$ scales linearly with the average of $\ln S$ in 2D systems. The spin conductance and spin thermopower for 1D NM/NM/FI systems are also studied in the presence of disorders. Largely speaking, the statistical properties of spin conductance in the 1D hybrid system are similar to that of charge transport in 1D normal metallic systems.

The remainder of this paper is organized as follows. Section II introduces the model Hamiltonian and the NEGF formula for the spin current in NM/NM/FI heterostructure. For readers not interested in the detailed formulation, Eq. (13) is used in the numerical simulation. Numerical results and discussion are presented in Sec. III, and followed by a conclusion in Sec. IV.

II. MODEL AND THEORETICAL FORMALISM

In this section, we describe our model and, using Keldysh theory, arrive at an expression for the spin current. The system considered in this study is shown in Fig. 1, whose Hamiltonian is

$$H = H_0 + H'. \quad (3)$$

H_0 is the unperturbed Hamiltonian, it consists of three parts: a left normal metal lead, a central normal metal region and a right ferromagnetic insulator lead,

$$H_0 = H_L + H_d + H_R. \quad (4)$$

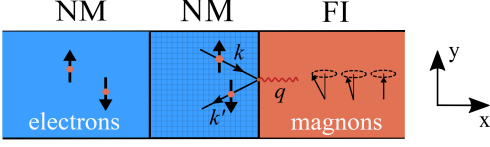


FIG. 1. Schematic view of the 2D NM/NM/FI system in consideration. A NM lead and a FI lead are connected to a central NM scattering area. In numerical calculations, Anderson-type disorder is added on the central scattering region. The x direction is the transport direction.

The left metallic lead Hamiltonian

$$H_L = \sum_{k\sigma} (\varepsilon_{k\sigma} - \mu_{L\sigma}) c_{k\sigma}^\dagger c_{k\sigma} \quad (5)$$

is described by noninteracting electrons, with $\mu_{L\sigma}$ the chemical potential for $\sigma = \{\uparrow, \downarrow\}$. The right ferromagnetic insulator lead is described by the Heisenberg model $H_R = -J \sum_{\langle ij \rangle} [\frac{1}{2} S_i^+ S_j^- + \frac{1}{2} S_i^- S_j^+ + S_i^z S_j^z]$, where S_i^\pm is the raising (lowering) operator for the localized spin at site i , S_i^z is the spin operator in z direction at site i and J is the exchange coupling. In low temperature limit, it can be approximated by free magnons⁷¹ ($\hbar = 1$):

$$H_R \simeq \sum_q \omega_q a_q^\dagger a_q, \quad (6)$$

where $a_q^\dagger (a_q)$ creates (annihilates) a magnon with momentum q and ω_q is the magnon dispersion given by material details. There is an extra factor $\sqrt{2S_0}$ associated with a_q and a_q^\dagger in H_{sd} which we dropped for the moment. Here S_0 is the length of the lattice spin. The central scattering region Hamiltonian is expressed as $H_d = \sum_{n\sigma} \varepsilon_{n\sigma} d_{n\sigma}^\dagger d_{n\sigma}$. In numerical calculations, the disorder is considered a random on-site potential U on the central scattering region. The coupling term H' is considered perturbatively on the basis of H_0 ,

$$H' = H_T + H_{sd}. \quad (7)$$

H_T is the coupling between left NM lead and central region,

$$H_T = \sum_{k\sigma n} \left[t_{k\sigma n} c_{k\sigma}^\dagger d_{n\sigma} + t_{k\sigma n}^* d_{n\sigma}^\dagger c_{k\sigma} \right]. \quad (8)$$

Following Ref. 72, the electron-magnon coupling between the central scattering region and right FI lead is described by the sd -type exchange interaction

$$H_{sd} = - \sum_{qnn'} J_{qnn'} \left[d_{n\uparrow}^\dagger d_{n'\downarrow} a_q^\dagger + d_{n'\downarrow}^\dagger d_{n\uparrow} a_q \right], \quad (9)$$

which describes a magnon-mediated spin-flipping scattering between states n and n' , by absorbing or emitting a magnon with momentum q . $J_{qnn'}$ is the scattering strength of the process, assumed to be weak and treated perturbatively to get the spin current in NEGF method. Note that we have neglected inelastic process such as electron-phonon interaction and other

relaxation processes and therefore focus on spin current at low temperatures.

When a temperature gradient ΔT across the NM/FI interface presents, a pure spin current is generated due to spin Seebeck effect⁴⁷⁻⁵². From current conservation rule, the spin current flows through this NM/NM/FI heterostructure equals the spin current flows through the right FI lead⁷³, which is given by

$$I_s = i \sum_{qnn'} J_{qnn'} [\langle d_{n\uparrow}^\dagger d_{n'\downarrow} a_q^\dagger \rangle - \langle a_q d_{n'\downarrow}^\dagger d_{n\uparrow} \rangle]. \quad (10)$$

In DC case, the spin current in this system is obtained in Keldysh theory as⁶¹

$$I_s = -i \int \frac{dE}{2\pi} \text{Tr} [D_{L\uparrow}(E) (\bar{\Sigma}_{R\uparrow}^<(E) - 2f_{L\uparrow}(E) \text{Im} \bar{\Sigma}_{R\uparrow}^a(E))], \quad (11)$$

where $D_{L\sigma} = G_\sigma^r \Gamma_{L\sigma} G_\sigma^a$ is the local DOS matrix for electron coming from the left lead⁷⁴, and the electron Green's function

$$G_\sigma^r = 1/[g_{d\sigma}^{-1} - \Sigma_{L\sigma}^r - \bar{\Sigma}_{R\sigma}^r] = 1/[G_{L\sigma}^{-1} - \bar{\Sigma}_{R\sigma}^r]. \quad (12)$$

In Born approximation (BA), the effective self-energy of right lead $\bar{\Sigma}_{R\uparrow}^<(t, t') = iG_{L\downarrow}^<(t, t') \Sigma_R^>(t', t)$, thus the DC spin current in BA is obtained

$$I_s = - \int \frac{d\omega}{2\pi} (f_R^B(\omega) - f_L^B(\omega)) \int \frac{dE}{2\pi} (f_{L\uparrow}(E) - f_{L\downarrow}(E + \omega)) \text{Tr} [A_R(E, \omega)], \quad (13)$$

with

$$A_R(E, \omega) = D_{L\uparrow}(E) D_{L\downarrow}^0(\bar{E}) \Gamma_R(\omega), \quad (14)$$

in which $\bar{E} = E + \omega$, f_R^B is Bose-Einstein distribution for the right lead, $f_{L\uparrow, \downarrow}$ is Fermi-Dirac distribution for the left lead, and f_L^B is an effective Bose-Einstein distribution for the left Fermion lead, defined as

$$f_L^B(\omega) = \frac{1}{e^{\beta_L(\omega + \Delta\mu_s)} - 1}. \quad (15)$$

$\beta_L = 1/k_B T_L$ is the inverse temperature of left lead, and $\Delta\mu_s = \mu_{L\uparrow} - \mu_{L\downarrow}$ is the spin bias applied on left NM lead. $D_{L\downarrow}^0 = G_{L\downarrow}^r \Gamma_{L\downarrow} G_{L\downarrow}^a$ is the partial local DOS matrix when the system is connected to the left lead only, $\Gamma_R = 2\text{Im} \Sigma_R^a$ is the linewidth function of right lead. The self-energy is formulated as

$$\bar{\Sigma}_{R\uparrow}^<(E) = \int \frac{d\omega}{2\pi} [f_R(\omega) G_{L\downarrow}^r(\bar{E}) + i f_{L\downarrow}(\bar{E}) \text{Im} G_{L\downarrow}^r(\bar{E})] \Gamma_R, \quad (16)$$

which is an energy convolution of local partial DOS with the spectral function of FI lead.

Following a similar procedure, we can easily get the spin current from left NM lead, from which it is readily shown that current conservation rule is satisfied.

III. NUMERICAL RESULTS AND DISCUSSION

In normal metallic systems without disorder, the conductance, proportional to the total transmission coefficient of incoming channels, is the quantity that measures the ability of transporting electrons. For magnon-mediated spin transport in our system, the right lead is an insulator, we do not have the concept of transmission coefficient, hence the spin conductance is used as a measure of spin transport.

In the linear response regime, we find spin current up to the second order in the electron-magnon coupling strength $J_{qn\prime}$,

$$I_s = G_T \Delta T - G_\mu \mu_s, \quad (17)$$

where G_T is the spin conductance driven by temperature gradient ΔT across the interface, G_μ is the spin conductance driven by spin bias μ_s in left metallic lead. In our numerical calculations, G_T and G_μ are determined by the spin current, $G_T = I_s/\Delta T$ when the spin bias is zero and the temperature bias ΔT is small. Similarly, $G_\mu = I_s/\mu_s$ when the temperature bias is zero and the spin bias is small. Analogous to the thermopower in thermoelectric studies, we can define a spin thermopower $S = \mu_s/\Delta T$. Here ΔT and μ_s are temperature bias and spin bias under which the generated spin currents cancel to each other. The spin thermopower measures the ability of the heterostructure to convert thermal gradient into spin accumulation in the metallic lead or vice versa. In the linear response regime it reduces to

$$S = \frac{G_T}{G_\mu}, \quad (18)$$

which is used in numerical calculations.

For simplicity, we consider the situation that the s-d interaction takes place only at the same site of the NM/FI interface, which leads to the simplification $J_{qn\prime} = J_{qn}\delta_{nn'}$. Without losing generality, the hybridization function between central region and the magnonic reservoir is assumed to be Ohmic and expressed as $\Gamma_R(\omega) = \pi\alpha t\omega e^{-\omega/\omega_c}$, here α is the effective coupling strength, ω_c is the cutoff frequency and t is the hopping constant in our tight-binding calculation.

Note the Hamiltonian Eq.(3) is formulated in momentum space, by using a finite difference procedure⁷⁵ we get its real-space form. When the disorder is present, an on-site potential energy from an uniform distribution of $[-W/2, W/2]$ is added to the Hamiltonian of the central scattering region, W is the disorder strength in unit of hopping constant t . More than 10000 disorder samples are collected in numerical calculations. A square lattice with lattice spacing $a = 5\text{nm}$ is used in tight-binding calculation, corresponding to a hopping constant $t = 21.768\text{meV}$. The whole calculations are carried out in Born approximation Eq.(13). The spin conductance G_T and spin thermopower S are in unit of $\mu\text{eV/K}$. We investigate the spin transport and scaling properties of 1D and 2D NM/NM/FI systems.

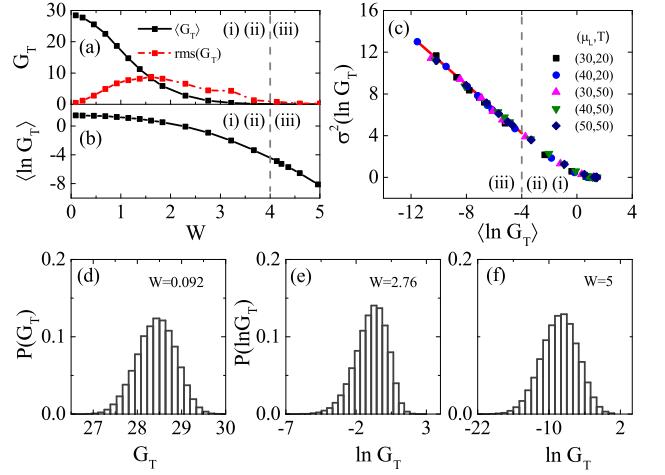


FIG. 2. (a) The average spin conductance $\langle G_T \rangle$ and its fluctuation $\text{rms}(G_T)$ as a function of disorder strength W for $\mu_L = 40\text{meV}$, $T = 50\text{K}$. (b) The average of logarithm of spin conductance G_T as a function of disorder strength W . Parameters are the same with (a). (c) The variance of $\ln G_T$ dependence on mean $\langle \ln G_T \rangle$ for different Fermi energies and temperatures. (d)–(f) Spin conductance distribution $P(G_T)$ and $P(\ln G_T)$ for $\mu_L = 40\text{meV}$, $T = 50\text{K}$ in three different disorder strength regimes. 40000 disorder samples are collected. The gray dashed line separates the diffusive regime (ii) and the localized regime (iii).

A. Spin transport and scaling in 1D NM/NM/FI system

For the 1D hybrid system, we use a central region of 30 chain sites and fix the cutoff frequency $\omega_c = 15\text{meV}$, and $\alpha = 0.1$. Two semi-infinite 1D leads are connected to the central region. In Fig. 2(a), the disorder-averaged spin conductance $\langle G_T \rangle$ and its fluctuation $\text{rms}(G_T)$ are depicted as a function of disorder strength W with Fermi energy $\mu_L = 40\text{meV}$ and temperature $T = 50\text{K}$. The spin conductance fluctuation is defined as

$$\text{rms}(G_T) = \sqrt{\langle G_T^2 \rangle - \langle G_T \rangle^2}, \quad (19)$$

in which $\langle \dots \rangle$ denotes the average over different disorder configurations for the same disorder strength W . It shows that $\langle G_T \rangle$ and $\text{rms}(G_T)$ are in the same order of magnitude similar to the situation of charge transport in normal systems. The behaviors of $\langle G_T \rangle$ and $\text{rms}(G_T)$ versus W are also similar to the charge conductance fluctuation in normal systems which allows us to identify three regimes: (i) metallic regime for small disorder W ; (ii) diffusive regime centered around $W \sim 1.5$; (iii) localized regime for $W \geq 4$. The corresponding regimes are labeled in Fig. 2(a)–(c) and separated by gray dashed line. Since the metallic regime is too narrow to be labeled, we have omitted it in figures. Fig. 2(b) shows the mean $\langle \ln G_T \rangle$ as a function of disorder strength W for the same μ_L and T .

The SPS for 1D non-interacting Fermi systems predicts that in the localized regime, the universal exponent $n = 1$ and the distribution of $\ln G$ is Gaussian. We show in Fig. 2(c) the variance $\sigma^2(\ln G_T)$ versus $\langle \ln G_T \rangle$ for different Fermi energies,

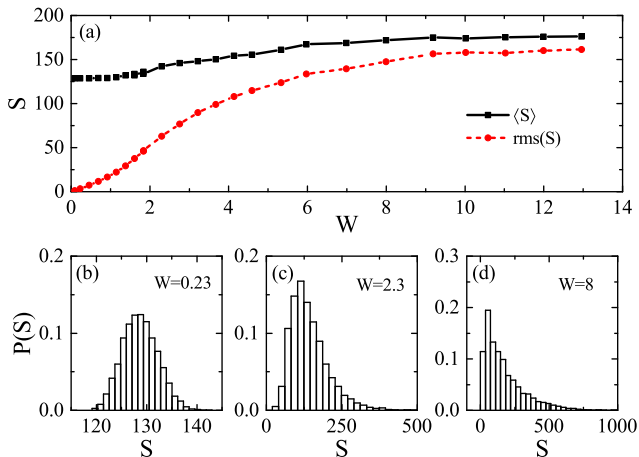


FIG. 3. (a) The average spin thermopower $\langle S \rangle$ and its fluctuation $\text{rms}(S)$ as a function of disorder strength W . (b)–(d) The histogram distribution of spin thermopower in different disorder strengths. System size: 1×30 , $\mu_L = 40\text{meV}$, $T = 50\text{K}$.

disorder strengths, and temperatures. We see that the data points collapse well into a single line in the localized regime, which is fitted to be

$$\sigma^2(\ln G_T) = -1.16\langle \ln G_T \rangle - 0.38. \quad (20)$$

The universal exponent $n = 1$. The distribution of spin conductance G_T and $\ln G_T$ is shown in Fig. 2 (d)–(f) at different disorder strengths. We see that in the metallic regime with $W = 0.092$, the distribution $P(G_T)$ is like a Gaussian. As disorder increases, the Gaussian distribution evolves into an asymmetric non-Gaussian distribution. For non-Gaussian distribution, the distribution of $\ln G_T$ is usually analyzed instead of G_T ^{76,77}. It shows a one-sided log-normal distribution in the diffusive regime at $W = 2.76$ and a log-normal distribution in larger disorder $W = 5$. Recall that in 1D normal systems, Gaussian distribution, one-sided log-normal distribution^{23–26,30}, and log-normal distribution^{25,26,78,79} were found for metallic, diffusive, and localized regimes, respectively. The universal exponent n together with the log-normal distribution suggests that SPS works in the localized regime. Therefore in 1D, statistical behavior of the magnon-mediated spin transport is consistent with that of charge transport in the normal metallic system in the presence of Anderson disorders.

The mean spin thermopower and its fluctuation is shown in Fig. 3(a). We observe that the mean $\langle S \rangle$ is slightly enhanced by disorder and approaches a finite constant in the localized regime. The fluctuation keeps the same order as $\langle S \rangle$ in the localized regime. Fig. 3(b)–(d) show the histogram distributions of spin thermopower. For weak disorder $W = 0.23$ in the metallic regime, the distribution function is nearly Gaussian. While increasing disorder, spin thermopower develops a long tail on the right side of the distribution.

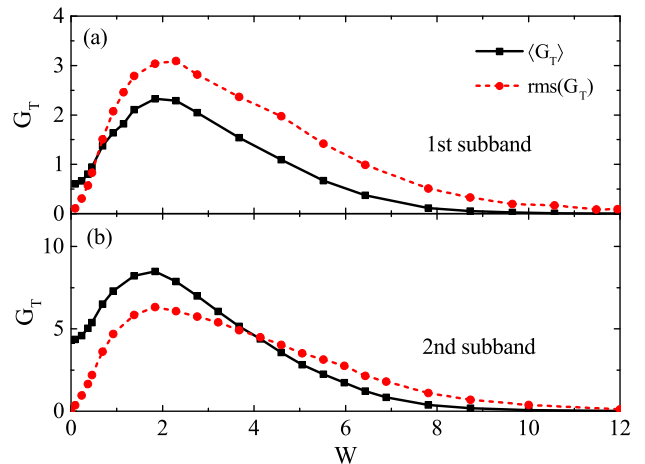


FIG. 4. The average conductance $\langle G_T \rangle$ and conductance fluctuation $\text{rms}(G_T)$ as a function of disorder strength W in the first (a) and second (b) subband of 2D NM/NM/FI. Parameters used are $\mu_L = \{0.9, 3\}\text{meV}$, $\omega_c = \{0.24, 0.2\}\text{meV}$, $T = 5\text{K}$, and lattice size: 20×20 .

B. Disorder-enhanced spin transport in 2D NM/NM/FI system

In 2D calculations, we consider a central scattering region of square lattice with size 20×20 ⁸⁰. Two leads (one normal metallic lead and one ferromagnetic insulating lead) with the same width as the lateral dimension of central region are considered as shown in 1. To reduce the computational complexity, we restrict the energies of incoming electrons from left lead to be in the first and second subbands. Since the choice of the effective coupling strength α should be applicable to real materials, we here choose the most used interface Pt/YIG with $\alpha = 10^3$, corresponding to $\eta = 10$ in Ref 72. The cutoff frequency for the first and second subbands are $\omega_c = 0.24\text{meV}$ and 0.2meV , so that the magnonic spectra decays nearly to zero at the edge of the subbands.

Fig. 4 depicts the average spin conductance $\langle G_T \rangle$ and its fluctuation $\text{rms}(G_T)$ in first and second subbands. It shows again that the average spin conductance and its fluctuation are in the same order of magnitude, similar to the situation of charge transport in normal metallic system. In 2D normal systems, disorder is known to suppress electron transport monotonically. While in 2D NM/NM/FI system the average spin conductance varies non-monotonically with increasing disorder strength. For the first subband calculation Fig. 4(a), $W = 0$ gives the spin conductance of clean system $G_T = 0.6$. When weak disorder is added to the system, the average spin conductance is enhanced. The largest enhancement, about 5 times, is reached around disorder strength $W = 2$. Further increasing disorder strength continuously suppresses the average spin conductance till the spin transport is completely blocked beyond $W = 12$. Fig. 4(b) shows the same calculations for the second subband, we see that all the behaviors remain the same except a smaller enhancement, which indicates that the spin conductance enhancement is a generic behavior.

The unusual disorder-enhancement behavior contrary to

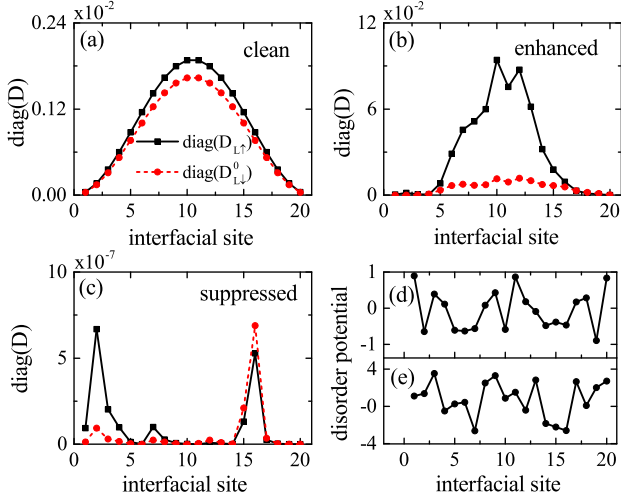


FIG. 5. (a) The diagonal matrix elements of $D_{L\uparrow}$ and $D_{L\downarrow}^0$ at the NM/FI interface for a particular energy and frequency $E = 1.26\text{meV}$ and $\omega = 0$ for 2D clean system. (b) The same as in panel (a) but for a disorder-enhanced configuration with $W = 2$. (c) The same as in panel (a) but for a disorder-suppressed configuration with $W = 7$, $E = 0.7\text{meV}$, $\omega = 0.1\text{meV}$. (d) and (e) are disorder potentials at the NM/FI interface of the corresponding configuration in (b) and (c) respectively. The potential is displayed in unit of t .

Anderson localization theory indicating that there is another mechanism dominating in the weak disorder regime. It can be seen from Eq. (14) that the quantity A_R thus the spin conductance is determined by $D_{L\uparrow}(E)$ and $D_{L\downarrow}^0(E)$, which are the local DOS matrices at the NM/FI interface. Hence, we attribute the disorder-enhancement behavior to the increase of DOS at interface. To confirm this, we examine in Fig. 5 the diagonal matrix element of the two matrices $D_{L\uparrow}(E)$ and $D_{L\downarrow}^0(E)$ at a typical energy and frequency. The local DOS of clean system ($W = 0$) for $E = 1.26\text{meV}$, $\omega = 0$ is shown in Fig. 5 (a). The spin conductance for clean system is $G_T = 0.6$. Fig. 5 (b) shows the DOS for a specific disorder configuration with strength $W = 2$, and an enhanced $G_T = 5.20$. Fig. 5 (c) depicts the same as panel (b) but with $W = 7$ and a suppressed $G_T = 1.30 \times 10^{-3}$, in which $E = 0.7\text{meV}$, $\omega = 0.1\text{meV}$ is chosen. Indeed, for a disorder-enhanced spin conductance the interfacial DOS is enhanced, while for a suppressed spin conductance the interfacial DOS is suppressed.

It is notable that the enhancement of average spin conductance occurs only in 2D systems. In 1D systems, there is only one site at the interface where the random potential is either positive or negative with equal probability. Since positive (negative) potential decreases (increases) the local DOS, on average there is no effect on self-energy of the right lead for 1D systems. For 2D systems, however, in any configuration, there are always some sites with negative potential at NM/FI interface (see Fig. 5 (d–e)) so that electrons can dwell around these sites leading to the enhancement of local DOS and hence the enhancement of the spin conductance in weak disorder. While further increasing disorder strength ($W > 2$),

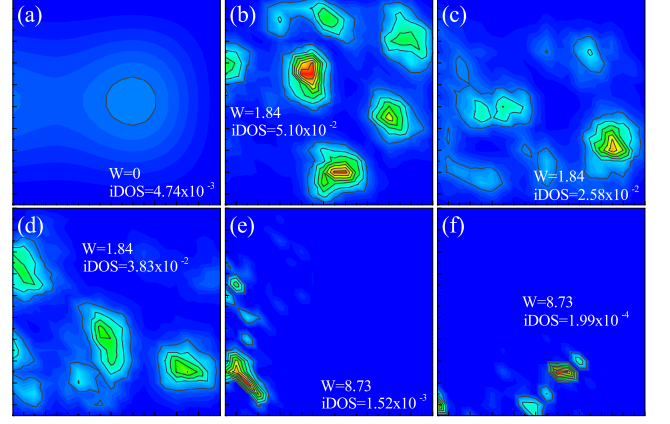


FIG. 6. The local DOS in the scattering region for 2D NM/NM/FI system with and without disorders. (a) DOS for the clean system. (b)–(d) DOS for three typical disorder configurations at weak disorder $W = 1.84$. (e)–(f) DOS for two typical disorder configurations at strong disorder $W = 8.73$. Here iDOS is the total interfacial DOS at NM/FI interface and we have used $\mu_L = 0.9\text{meV}$, $T = 5\text{K}$.

the localized state induced by strong disorder dominates, the average spin conductance is suppressed. These two competing contributions lead to the non-monotonic line shape in average spin conductance. Calculation of spin conductance in this system found that an enhancement of nearly three orders of magnitude can be achieved by engineering the interfacial potentials⁶¹, which is consistent with our results.

As we discussed above that the interfacial DOS is a major factor in spin conductance enhancement. What is the role played by the disorder in the scattering region rather than the interface? In the presence of Anderson disorders, local potential $U = [-W/2, W/2]$ can be negative. That will trap the electron, leading to an increasing of dwell time or local DOS. Thus there are many peaks in local DOS landscape. As a result, the interfacial DOS increases whenever these peaks are near the interface. In Fig. 6(b)–(d), we show typical local DOS landscape for $W = 1.84$ where the enhancement of average spin conductance is near its maximum. Comparing with the clean system Fig. 6(a), the total interfacial DOS is increased by a factor of 11, 5, 8 for Fig. 6(b)–(d), respectively, which is responsible for the enhancement of average spin conductance. For larger disorders $W = 8.73$ (Fig. 6(e)–(f)), the electron wave function is more localized with peaks of local DOS much sharper. In addition, it is much more difficult for electron to reach the NM/FI interface in the strong disorders. Therefore, the total interfacial DOS decreases drastically and enhancement does not occur.

The average spin thermopower $\langle S \rangle$ and its fluctuation $\text{rms}(S)$ for 2D NM/NM/FI system is shown in Fig. 7(a). Parameters are $\mu_L = 0.9\text{meV}$, $T = 5\text{K}$. Different from 1D case, the average spin thermopower varies non-monotonically while increasing disorder and approaches to a finite constant 18.3 in the localized limit. $\langle S \rangle$ has a local minimum at $W = 1$. The fluctuation is in the same order as the average spin thermopower and saturates in strong disorder limit. Distributions of spin thermopower are shown in Fig. 7(b)–(d).

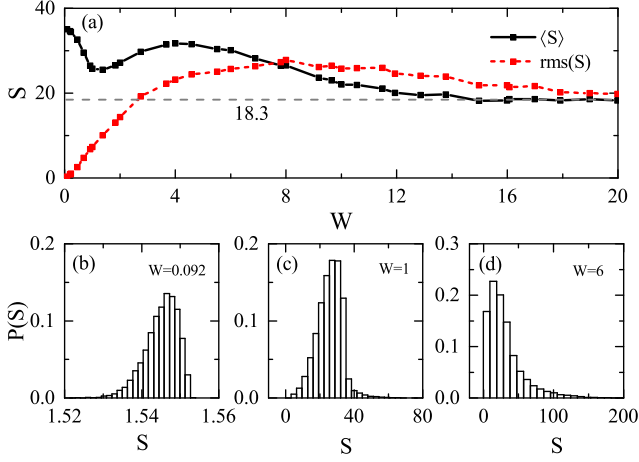


FIG. 7. The spin thermopower for 2D NM/NM/FI system. (a) The mean $\langle S \rangle$ and fluctuation $\text{rms}(S)$ as a function of disorder strength. (b)–(d) Histogram distributions of S for specific disorder strengths. $\mu_L = 0.9\text{meV}$, $T = 5\text{K}$.

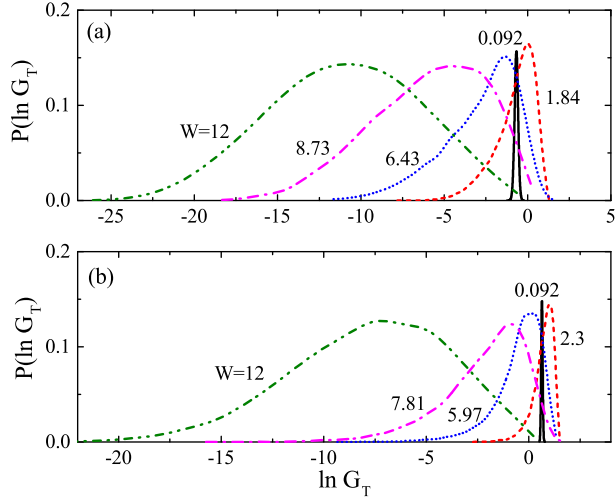


FIG. 8. Spin conductance distribution $P(\ln G_T)$ of 2D system for different disorder strength W in first subband (a) and second subband (b). Parameters are the same with Fig. 4.

For $W < 1$ the distribution Fig. 7(b) has a long tail on the left side (small S), indicating a negative skewness. While for $W > 1$ the distribution Fig. 7(d) has long tail on the right side (large S), indicating a positive skewness. For disorder strength $W = 1$, the distribution is nearly symmetric.

C. Scaling behaviors in 2D NM/NM/FI system

We first investigate the spin conductance distribution in 2D NM/NM/FI system. Fig. 8 shows the distribution for different disorder strength in first subband and second subband. In the first subband, when the disorder strength is small ($W = 0.092$), the distribution $P(G_T)$ is like Gaussian. For

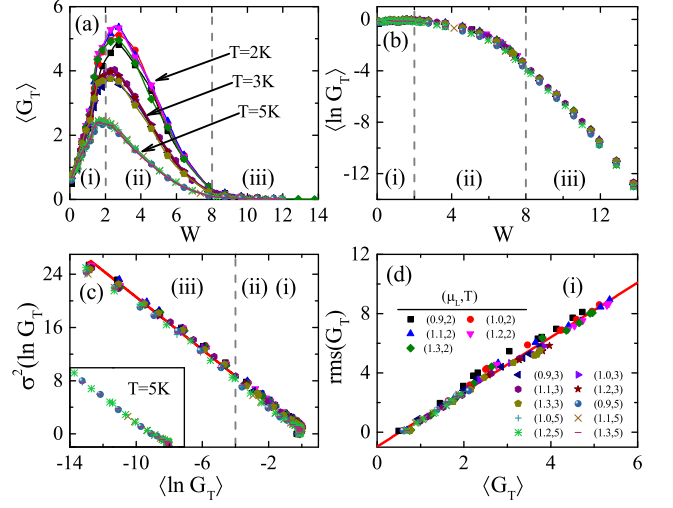


FIG. 9. Statistics of spin conductance for Fermi energies $\mu_L = \{0.9, 1.0, 1.1, 1.2, 1.3\}\text{meV}$ and temperatures $T = \{2, 3, 5\}\text{K}$. Figure legend is shown in (d). The gray dashed lines separate three different regimes: (i) the metallic regime, (ii) the diffusive regime and (iii) the localized regime. (a) Average spin conductance as a function of disorder strength W . (b) Average logarithm of spin conductance dependence of disorder strength. (c) Scaling of $\ln G_T$ variance on average $\ln G_T$ in the localized regime. Inset: Data for $T = 5\text{K}$ and different Fermi energies are selected. (d) Scaling of spin conductance fluctuation on average spin conductance in the metallic regime.

intermediate disorders $W = 1.84, 6.43, 8.73$, the distribution $P(G_T)$ follows a one-sided log-normal. While in the strong disorder region $W \simeq 12$, the distribution $P(\ln G_T)$ is found to be a nearly Gaussian. The distribution in the second subband is quite similar to that of the first subband. Although these findings are similar to the results in 2D normal system⁷⁹, we note that the details are different though, which is manifested in the scaling behaviors. The peak positions of line $W = 1.84$ and $W = 2.3$ in Fig. 8 (a) and (b) lie to the right of line $W = 0.092$. This corresponds to the weak disorder regime where the average spin conductance is enhanced ($W < 2$ in Fig. 4).

We next study the scaling properties of 2D NM/NM/FI system. The mean $\langle G_T \rangle$, $\langle \ln G_T \rangle$, variance $\sigma^2(\ln G_T)$ and fluctuation $\text{rms}(G_T)$ of different Fermi energies and temperatures are shown in Fig. 9.

The average spin conductance for different Fermi energies $\mu_L = \{0.9, 1.0, 1.1, 1.2, 1.3\}\text{meV}$ and temperatures $T = \{2, 3, 5\}\text{K}$ are plotted in Fig. 9(a). Note that all the Fermi energies locate in the first subband. We observe disorder-enhancement behavior in weak disorder for all parameters. Moreover, the system has larger average spin conductance and stronger fluctuation at lower temperature. Raising temperature suppresses the average spin conductance and its fluctuation. Fig. 9(b) shows the average of the logarithm of spin conductance $\langle \ln G_T \rangle$ as a function of disorder strength. It is interesting that $\langle \ln G_T \rangle$ collapse to a single curve for different Fermi energies and temperatures, indicating that disorder strength can also be used to scale $\langle \ln G_T \rangle$.

Previous scaling study for charge transport in 2D normal system has shown that in the localized regime, the variance of charge conductance $\sigma^2(\ln G)$ versus $\langle \ln G \rangle$ have a power-law dependence with an exponent $n = 2/3$ ³⁵. We examine relation Eq.(2) for 2D NM/NM/FI system in Fig. 9(c). We see that data points for $\langle \ln G_T \rangle < -4$, or equivalently $W > 8$, collapse onto a universal line (red line) well-fitted by

$$\sigma^2(\ln G_T) = -1.98\langle \ln G_T \rangle - 0.75. \quad (21)$$

The inset depicts the variance dependence on mean $\langle \ln G_T \rangle$ for a specific temperature $T = 5\text{K}$, which shows even better linear behavior. We conclude that for 2D NM/NM/FI system in the localized regime, universal relation Eq.(2) is justified with $n = 1$ and the scaling weakly depends on temperature.

For the region out of localized regime, it is difficult to study the scaling properties using $\ln G_T$ since data points is scattered for large $\langle \ln G_T \rangle$. However, using $\langle G_T \rangle$ and its fluctuation $\text{rms}(G_T)$, we find an additional scaling behavior in the weak disorders. The $\text{rms}(G_T)$ dependence on average spin conductance for $W < 2$ is plotted in Fig. 9(d). The data points collapse well onto the red line, fitted by

$$\text{rms}(G_T) = 1.84\langle G_T \rangle. \quad (22)$$

Note that at weak disorders, the charge (spin) conductance fluctuation always increases with increasing of disorder since there is no fluctuation when disorder is zero. The positive slope indicates that the average spin conductance increases with disorder strength, i.e., enhancement of spin conductance at weak disorders.

As discussed above, our calculation enables us to verify three regimes in this 2D NM/NM/FI system. (i) The metallic regime for $W < 2$, where the average spin conductance is enhanced due to the large DOS at the NM/FI interface when increasing disorder strength. The spin conductance fluctuation can be linearly scaled by mean $\langle G_T \rangle$. (ii) The diffusive regime for $2 < W < 8$, where localization caused by disorders in the entire scattering region strongly competes with interfacial resonance, leading to a non-monotonic average spin conductance. (iii) The localized regime for $W > 8$, in which Anderson localization dominates. The variance $\sigma^2(\ln G_T)$ for different disorder strengths, Fermi energies can be linearly scaled by the mean $\langle \ln G_T \rangle$. The three regimes are labeled in Fig. 9 and separated by gray dashed lines. Calculations in the second subband show similar results.

Since the distribution $P(\ln G_T)$ in the localized regime is nearly Gaussian, we examine its deviation from Gaussian distribution by calculating the skewness, kurtosis and lowest non-trivial cumulants of $\ln G_T$.

The definitions of the third and fourth cumulants κ_3, κ_4 , skewness γ_1 and kurtosis γ_2 used here are the same as those defined in Ref. 79 and 81 with $\kappa_3 = \mu_3, \kappa_4 = \mu_4$, and

$$\gamma_1 = \frac{\mu_3}{\mu_2^{3/2}}, \quad (23)$$

$$\gamma_2 = \frac{\mu_4}{\mu_2^2} - 3. \quad (24)$$

Here $\mu_m = \langle (x - \langle x \rangle)^m \rangle$ is the m -th order central moment. Skewness is usually used to quantify the degree of asymmetry

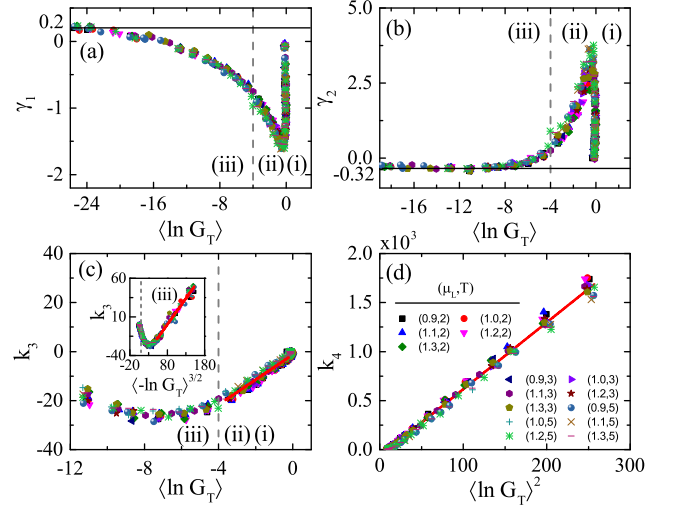


FIG. 10. Skewness γ_1 , kurtosis γ_2 , third and fourth cumulants k_3, k_4 of $\ln G_T$ distribution for 2D NM/NM/FI system in the first subband, parameters are the same as in Fig. 9. The legend is shown in (d). The gray dashed lines separate the localized regime from diffusive and metallic regime in (a)–(c). The inset of (c) shows k_3 versus $\langle -\ln G_T \rangle^{3/2}$.

of a distribution. It is positive when the distribution has a long flat tail in larger values, while a zero skewness indicates that the distribution is symmetric about its mean value. Kurtosis is a measure of sharpness or flatness of a distribution. It is zero for a Gaussian distribution, greater than zero if the distribution has a sharper peak compared to a normal distribution and less than zero if the distribution peak is flatter.

The skewness, kurtosis, third and fourth cumulants of $\ln G_T$ are depicted in Fig. 10 for different Fermi energies and temperatures in the first subband, showing universal behaviors. The same set of parameters are used as in Fig. 9. In the localized regime skewness and kurtosis approach to nonzero values 0.2 and -0.32 , respectively (see horizontal line in Fig. 10(a)(b)). Thus the $\ln G_T$ distribution in localized regime is not Gaussian. The third cumulant in Fig. 10(c) shows a good linear dependence on $\langle \ln G_T \rangle$ in the diffusive regime. The linear dependence is denoted by the red line and described by $k_3 = 5.11\langle \ln G_T \rangle - 1.26$. But in the localized regime, k_3 is approximately scaled as $\langle -\ln G_T \rangle^{3/2}$ (see inset of Fig. 10(c)). In addition, the fourth cumulant k_4 scales linearly with $\langle \ln G_T \rangle^2$ in all three regimes and shows weak dependence on temperature (Fig. 10(d)),

$$k_4 = 6.81\langle \ln G_T \rangle^2 - 65.46. \quad (25)$$

In Fig. 10(d), we use meVK^{-1} as the unit of spin conductance. Note that the universal behaviors of higher order moments or cumulants (third and fourth) for charge transport have been investigated before in the localized regime with the following result: $\kappa_3 \sim \langle -\ln G \rangle$ and $\kappa_4 \sim \langle -\ln G \rangle^{4/3}$ in 2D normal metallic systems⁸².

From the universal behaviors of moments of $\langle \ln G_T \rangle$ in the localized regime, we anticipate the distribution of spin conductance mediated by magnon may also exhibit univer-

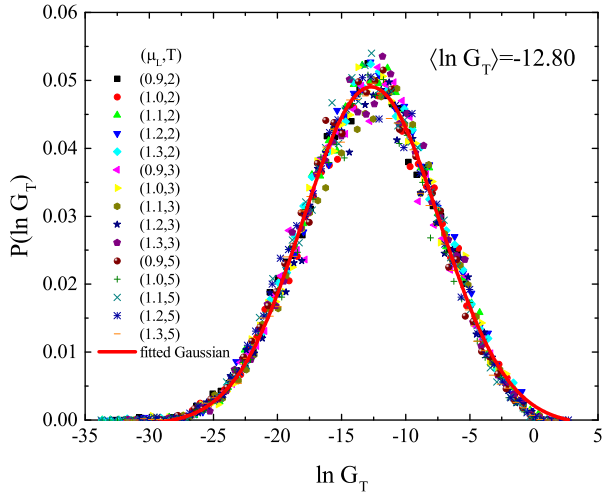


FIG. 11. The distribution of $\ln G_T$ versus $\ln G_T$ for fixed $\langle \ln G_T \rangle = -12.80$ but for different Fermi energies and temperatures in the localized regime with $W = 13.78$. The curve is fitted using a Gaussian. The deviation is due to the higher order cumulants.

sal behavior in the same regime. Indeed, as shown in Fig. 11, different data with the same $\langle \ln G_T \rangle$ approximately collapse on a single curve, suggesting that the distribution $P(\ln G_T, \langle \ln G_T \rangle)$ is a universal function. The curve is fitted using a Gaussian. The deviation from Gaussian is accounted for the higher order cumulants.

Note that the Fermi energies used in scaling analysis (Fig. 9 and Fig. 10) are near the center of the first subband, this is the region where SPS works in normal system²⁰. Although the range of Fermi energies and temperature is not very wide, the spin conductance in Fig. 9(a) varies large enough in magnitude to support our scaling analysis.

Finally, we examine the statistical behavior of the spin thermopower. In Fig. 12(a), $\langle \ln S \rangle$ versus disorder strength W are plotted for different Fermi energies and temperatures. We see that data collapse onto three different curves and each curve corresponds to a fixed temperature. If we shift each curve vertically, they will collapse roughly on a single curve especially in the localized regime (see Fig. 12(b)). In Fig. 12(c), we depict the variance of $\ln S$ as a function of $\langle \ln S \rangle$ which seems to show three curves. Note that in Fig. 12(a), the boundary of localized regime is $W = 8$ and this corresponds to different boundaries for $\langle \ln S \rangle$ which are $\langle \ln S \rangle \approx 1.56, 1.37, 1.18$, respectively for $T = 2, 3, 5$ K. In Fig. 12(c), three dashed vertical lines correspond to these boundaries of localized regime. If we shift each curve horizontally, three curves can approximately collapse onto a single curve in the localized regime as shown in Fig. 12(d). This suggests that $\sigma^2(\ln S) = a\langle \ln S \rangle + b$ where $a = -1.17$ is a universal constant and b depends only on the temperature.

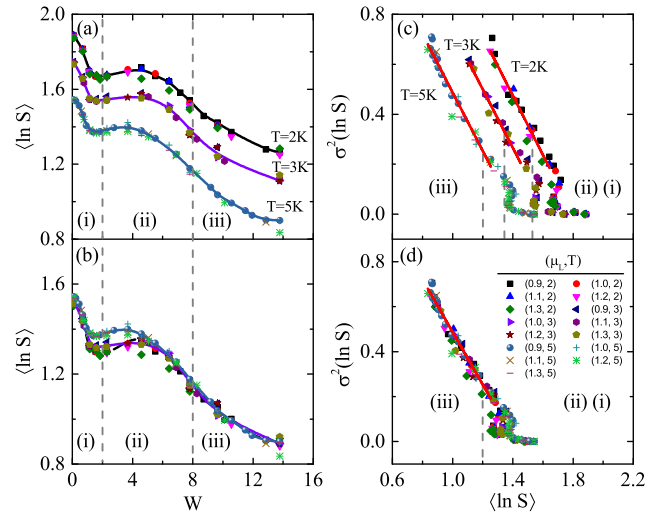


FIG. 12. The scaling of average and variance of $\ln S$ in the presence of disorders. (a) $\langle \ln S \rangle$ versus W for different Fermi energies and temperatures. (b) The same as (a) but the curves for $T = 2, 3$ K are shifted vertically by 0.37 and 0.22, respectively. (c) The variance of $\ln S$ versus $\langle \ln S \rangle$ for different Fermi energies and temperatures. Three vertical dashed lines mark the boundaries between localized and diffusive regimes, respectively, for different temperatures. (d) The same as (c) but the curves for $T = 2, 3$ K are shifted horizontally so that three boundaries between localized and diffusive regimes coincide.

IV. CONCLUSION

We have numerically investigated the magnon-mediated spin transport in disordered 1D and 2D NM/NM/FI heterostructures based on the NEGF method. Disorder in 1D NM/NM/FI systems was found to continuously suppress the average spin conductance and the spin conductance distribution is in good agreement with that of the charge transport in 1D NM systems. In 2D NM/NM/FI systems, the averaged spin conductance is enhanced at weak disorder and suppressed at strong disorder. This non-monotonic behavior is attributed to the competition between resonance at NM/FI interface and localization of electrons in the central scattering region. The resonance originates from the fact that electron-magnon coupling in this system is given by an energy convolution of interfacial DOS.

The scaling properties of spin conductance were also studied. For both 1D and 2D NM/NM/FI systems, it was found that the variance of logarithm of spin conductance varies linearly with the average of logarithm of spin conductance $\langle \ln G_T \rangle$ in the localized regime which is universal, independent of system parameters such as Fermi energy, disorder strength and temperature. For 2D NM/NM/FI system, the scaling behavior of spin conductance is different from the $2/3$ power-law found for charge transport in 2D normal systems²⁰. The third and fourth order cumulants of $\ln G_T$ versus $\langle \ln G_T \rangle$ were found to follow a universal function in the whole range of W . In particular, we found the universal behavior $k_n \sim \langle -\ln G_T \rangle^{\alpha_n}$ in the localized regime with $\alpha_n = 3/2, 2$, re-

spectively, for $n = 3, 4$. The distribution of $\ln G_T$ in the localized regime is not Gaussian but was found to be a universal function that depends only on $\langle \ln G_T \rangle$. Moreover, we found an additional scaling in the metallic regime. In this regime, the spin conductance fluctuation $\text{rms}(G_T)$ scales linearly with its average $\langle G_T \rangle$. Finally, the statistical property of spin thermopower S was investigated and the variance of $\ln S$ versus $\langle \ln S \rangle$ was found to obey a linear scaling relation in the localized regime. Our 2D results suggest that the magnon mediated spin transport in the presence of disorders belongs to

a different universality class from that of charge transport in NM systems.

ACKNOWLEDGMENTS

This work was financially supported by the Natural Science Foundation of China (Grant No.12034014 and No.12174262).

-
- * jianwang@hku.hk
- ¹ P. W. Anderson, Phys. Rev. 109, 1492 (1958).
 - ² B. Kramer, A. MacKinnon, Rep. Prog. Phys. 56 1469 (1993).
 - ³ E. Abrahams, 50 Years of Anderson Localization (World Scientific, Singapore, 2010).
 - ⁴ N. F. Mott, J. Non-Cryst. Solids 1, 1 (1968).
 - ⁵ J. T. Edwards, D. J. Thouless, J. Phys. C 5, 807 (1972).
 - ⁶ E. Abrahams, P. W. Anderson, D. C. Licciardello, and T. V. Ramakrishnan, Phys. Rev. Lett. 42, 673 (1979).
 - ⁷ P. W. Anderson, D. J. Thouless, E. Abrahams, D. S. Fisher, Phys. Rev. B 22, 3519 (1980).
 - ⁸ B. Shapiro, Ann. Israel Phys. Soc. 5, 367 (1983).
 - ⁹ B. Shapiro, Phil. Mag. B 56, 1031 (1987).
 - ¹⁰ C. A. Müller, D. Delande, arXiv:1005.0915 (2010).
 - ¹¹ F. Wegner, Z. Phys. B 25, 327 (1976).
 - ¹² Y. Imry, Phys. Rev. Lett. 44, 469 (1980).
 - ¹³ P. A. Lee and A. D. Stone, Phys. Rev. Lett. 55, 1622 (1985).
 - ¹⁴ A. D. Stone and P. A. Lee, Phys. Rev. Lett. 54, 1196 (1985).
 - ¹⁵ Y. Imry, EPL 1, 249 (1986).
 - ¹⁶ P. A. Lee, A. D. Stone and H. Fukuyama, Phys. Rev. B 35, 039 (1987).
 - ¹⁷ K. A. Muttalib, J. L. Pichard and A. D. Stone, Phys. Rev. Lett. 59, 2475 (1987).
 - ¹⁸ J. L. Pichard, M. Sanquer, K. Slevin, and P. Debray, Phys. Rev. Lett. 65, 1812 (1990).
 - ¹⁹ J. L. Pichard and M. Sanquer, Physica A 167 66 (1990).
 - ²⁰ J. Prior, A. M. Somoza, and M. Ortuno, Phys. Rev. B 72, 024206 (2005).
 - ²¹ A. La Magna, I. Deretzis, G. Forte, and R. Pucci, Phys. Rev. B 78, 153405 (2008).
 - ²² A. La Magna, I. Deretzis, G. Forte, and R. Pucci, Phys. Rev. B 80, 195413 (2009).
 - ²³ O. N. Dorokhov, JETP Lett. 36, 318 (1982).
 - ²⁴ P. A. Mello, P. Pereyra, and N. Kumar, Ann. Phys. (N.Y.) 181, 290 (1988).
 - ²⁵ V. Plerou and Z.Q. Wang, Phys. Rev. B 58, 1967 (1998).
 - ²⁶ K. A. Muttalib and P. Wolffe, Phys. Rev. Lett. 83, 3013 (1999).
 - ²⁷ P. J. Roberts, J. Phys.: Condens. Matter 4, 7795 (1992).
 - ²⁸ L. I. Deych, A. A. Lisyansky, and B. L. Altshuler, Phys. Rev. Lett. 84, 2678 (2000).
 - ²⁹ L. I. Deych, A. A. Lisyansky, and B. L. Altshuler, Phys. Rev. B 64, 224202 (2001).
 - ³⁰ A. Garcia-Martin and J. J. Saenz, Phys. Rev. Lett. 87, 116603 (2001).
 - ³¹ L. I. Deych, M. V. Eremenchouk, and A. A. Lisyansky, Phys. Rev. B 67, 024205 (2003).
 - ³² A. MacKinnon and B. Kramer, Phys. Rev. Lett. 47, 1546 (1981).
 - ³³ A. MacKinnon, B. Kramer, Z. Phys. B 53, 1 (1983).
 - ³⁴ M. Schreiber and M. Ottomeier, J. Phys.: Condens. Matter 4, 1959 (1992).
 - ³⁵ A. M. Somoza, M. Ortuno, and J. Prior, Phys. Rev. Lett. 99, 116602 (2007).
 - ³⁶ J. Prior, A. Somoza, and M. Ortuno, Eur. Phys. J. B 70, 513 (2009).
 - ³⁷ A. M. Somoza, J. Prior, M. Ortuno, and I. V. Lerner, Phys. Rev. B 80, 212201 (2009).
 - ³⁸ A. M. Somoza, P. Le Doussal, and M. Ortuno, Phys. Rev. B 91, 155413 (2015).
 - ³⁹ J. W. Kantelhardt and A. Bunde, Phys. Rev. B 66, 035118 (2002).
 - ⁴⁰ S. L. A. de Queiroz, Phys. Rev. B 66, 195113 (2002).
 - ⁴¹ In Ref. 20, $\ln R$ is used instead of $\ln G$. Note the resistance R is the inverse of conductance G , then we have $\langle \ln G \rangle = -\langle \ln R \rangle$ thus the same result is obtained.
 - ⁴² A. Brataas, B. van Wees, O. Klein, G. de Loubens, and M. Viret, Physics Reports, 885 (2020).
 - ⁴³ Y. Tserkovnyak, A. Brataas, and G. E. W. Bauer, Phys. Rev. B 66, 224403 (2002).
 - ⁴⁴ Y. Tserkovnyak, A. Brataas, G. E. W. Bauer, and B. I. Halperin, Rev. Mod. Phys. 77, 1375 (2005).
 - ⁴⁵ A. Azevedo, L. H. Vilela Leão, R. L. Rodriguez-Suarez, A. B. Oliveira, and S. M. Rezende, J. Appl. Phys. 97, 10C715 (2005).
 - ⁴⁶ E. Saitoh, M. Ueda, H. Miyajima, and G. Tatara, Appl. Phys. Lett. 88, 182509 (2006).
 - ⁴⁷ K. Uchida, S. Takahashi, K. Harii, J. Ieda, W. Koshibae, K. Ando, S. Maekawa, and E. Saitoh, Nature 455, 778 (2008).
 - ⁴⁸ K. Uchida, J. Xiao, H. Adachi, J. Ohe, S. Takahashi, J. Ieda, T. Ota, Y. Kajiwara, H. Umezawa, H. Kawai, G. E. W. Bauer, S. Maekawa, and E. Saitoh, Nat. Mater. 9, 894 (2010).
 - ⁴⁹ K. Uchida, M. Ishida, T. Kikkawa, A. Kirihara, T. Murakami, and E. Saitoh, J. Phys.: Condens. Matter 26, 343202 (2014).
 - ⁵⁰ G. E. W. Bauer, E. Saitoh, and B. J. van Wees, Nat. Mater. 11, 391 (2012).
 - ⁵¹ H. Adachi, K. Uchida, E. Saitoh, and S. Maekawa, Rep. Prog. Phys. 76, 036501 (2013).
 - ⁵² S. R. Boona, R. C. Myers, and J. P. Heremans, Energy Environ. Sci. 7, 885 (2014).
 - ⁵³ J. Xiao, G. E. Bauer, K. C. Uchida, E. Saitoh and S. Maekawa, Phys. Rev. B 81, 214418 (2010).
 - ⁵⁴ Y. Ohnuma, H. Adachi, E. Saitoh, and S. Maekawa, Phys. Rev. B 87, 014423 (2013).
 - ⁵⁵ Hua-Hua Fu, Dan-Dan Wu, L. Gu, M. Wu, and R. Wu, Phys. Rev. B 92, 045418 (2015).
 - ⁵⁶ H. Wu, L. Huang, C. Fang, B. S. Yang, C. H. Wan, G. Q. Yu, J. F. Feng, H. X. Wei, and X. F. Han, Phys. Rev. Lett. 120, 097205 (2018).
 - ⁵⁷ B. F. Miao, S. Y. Huang, D. Qu, and C. L. Chien, Phys. Rev. Lett. 111, 066602 (2013).

- ⁵⁸ G.M. Tang, X.B. Chen, J. Ren, and J. Wang, *Phys. Rev. B* 97, 081407 (2018).
- ⁵⁹ M. F. Jakobsen, A. Qaiumzadeh, and A. Brataas, *Phys. Rev. B* 100, 134431 (2019).
- ⁶⁰ Liupeng Yang, Yaoyu Gu, Lina Chen, Kaiyuan Zhou, Qingwei Fu, Wenqiang Wang, Liyuan Li, Chunjie Yan, Haotian Li, Like Liang, Zishuang Li, Yong Pu, Youwei Du, and Ronghua Liu, *Phys. Rev. B* 104, 144415 (2021).
- ⁶¹ G. Li, H. Jin, Y. Wei, J. Wang, arXiv:2112.11021.
- ⁶² F. Hellman et al., *Rev. Mod. Phys.* 89, 025006 (2017).
- ⁶³ Z. Qiu, K. Ando, K. Uchida, Y. Kajiwara, R. Takahashi, H. Nakayama, T. An, Y. Fujikawa, and E. Saitoh, *Appl. Phys. Lett.* 103, 092404 (2013).
- ⁶⁴ A. Aqeel, I. J. Vera-Marun, B. J. van Wees, and T. T. M. Palstra, *J. Appl. Phys.* 116, 153705 (2014).
- ⁶⁵ S. K. Lee, W. Y. Lee, T. Kikkawa, C. T. Le, M. S. Kang, G. S. Kim, A. D. Nguyen, Y. S. Kim, N. W. Park, and E. Saitoh, *Ad. Func. Mater.* 30, 2003192 (2020).
- ⁶⁶ V. Kalappattil, R. Geng, R. Das, M. Pham, H. Luong, T. Nguyen, A. Popescu, L. M. Woods, M. Klaui, H. Srikanth, and M. H. Phan, *Materials Horizons* 7, 1413 (2020).
- ⁶⁷ W. Y. Lee, N. W. Park, M. S. Kang, G. S. Kim, H. W. Jang, E. Saitoh, and S. W. Lee, *J. Phys. Chem. Lett.* 11, 5338 (2020).
- ⁶⁸ W. Y. Lee, N. W. Park, G. S. Kim, M. S. Kang, J. W. Choi, K. Y. Choi, H. W. Jang, E. Saitoh, and S. W. Lee, *Nano Lett.* 21, 189 (2021).
- ⁶⁹ H. L. Wang, C. H. Du, P. C. Hammel, and F. Y. Yang, *Phys. Rev. Lett.* 113, 097202 (2014).
- ⁷⁰ W. W. Lin, K. Chen, S. F. Zhang, and C. L. Chien, *Phys. Rev. Lett.* 116, 186601 (2016).
- ⁷¹ T. Holstein and H. Primakoff, *Phys. Rev.* 58, 1098 (1940).
- ⁷² J.S. Zheng, S. Bender, J. Armitis, R. E. Troncoso, and R. A. Duine, *Phys. Rev. B* 96, 174422 (2017).
- ⁷³ J. Ren, *Phys. Rev. B* 88, 220406 (2013).
- ⁷⁴ T. Christen and M. Buttiker, *Phys. Rev. Lett.* 77, 143 (1996).
- ⁷⁵ S. Datta, *Electronic Transport in Mesoscopic Systems* (Cambridge University Press, New York, 1995), Chapter 3.
- ⁷⁶ V. I. Melnikov, *Fiz. Tverd. Tela (Leningrad)* 23, 782 (1981)[*Sov. Phys. Solid State* 23, 444 (1981)].
- ⁷⁷ A. A. Abrikosov, *Solid State Commun.* 37, 997 (1981).
- ⁷⁸ M. Janssen, *Phys. Rep.* 295, 1 (1998).
- ⁷⁹ W. Ren, J. Wang, and Z.S. Ma, *Phys. Rev. B* 72, 195407 (2005).
- ⁸⁰ In contrast to the normal systems, when calculating spin conductance for one specific disorder sample, one has to perform a double integration (see Eq.(13)). In the calculation, we have chosen grid points 50×50 which amounts to an increase of computational load by a factor of 2500 comparing with the charge conductance calculation in NM systems.
- ⁸¹ P. Mohanty and R. A. Webb, *Phys. Rev. Lett.* 88, 146601 (2002).
- ⁸² A. M. Somoza, J. Prior, and M. Ortuno, *Phys. Rev. B* 73, 184201 (2006).